International Journal of Nanomedicine

Dovepress
open access to scientific and medical research

Open Access Full Text Article

ORIGINAL RESEARCH

# Effects of hydrogenated $TiO_2$ nanotube arrays on protein adsorption and compatibility with osteoblast-like cells

This article was published in the following Dove Press journal:
International Journal of Nanomedicine

International Journal of Nanomedicine downloaded from https://www.dovepress.com/
For personal use only.

Ran Lu,[1–3,*] Caiyun Wang,[1–3,*] Xin Wang,[1] Yuji Wang,[3] Na Wang,[1] Joshua Chou,[4] Tao Li,[1,2] Zhenting Zhang,[1] Yunhan Ling,[2] Su Chen[1]

[1]Laboratory of Biomaterials and Biomechanics, Beijing Key Laboratory of Tooth Regeneration and Function Reconstruction, School of Stomatology, Capital Medical University, [2]Laboratory of Advanced Functional Materials, Department of Materials Science and Engineering, Tsinghua University, [3]School of Pharmaceutical Sciences, Capital Medical University, Beijing, People's Republic of China; [4]Advanced Tissue Regeneration and Drug Delivery Group, School of Life Sciences, University of Technology Sydney, Sydney, NSW, Australia

*These authors contributed equally to this work

**Background:** Modified titanium (Ti) substrates with titanium dioxide ($TiO_2$) nanotubes have broad usage as implant surface treatments and as drug delivery systems.

**Methods:** To improve drug-loading capacity and accelerate bone integration with titanium, in this study, we hydrogenated anodized titanium dioxide nanotubes (TNTs) by a thermal treatment. Three groups were examined, namely: hydrogenated TNTs ($H_2$-TNTs, test), unmodified TNTs (air-TNTs, control), and Ti substrates (Ti, control).

**Results:** Our results showed that oxygen vacancies were present in all the nanotubes. The quantity of -OH groups greatly increased after hydrogenation. Furthermore, the protein adsorption and loading capacity of the $H_2$-TNTs were considerably enhanced as compared with the properties of the air-TNTs ($P<0.05$). Additionally, time-of-flight secondary ion mass spectrometry (TOF-SIMS) was used to investigate the interactions of TNTs with proteins. During the protein-loading process, the $H_2$-TNTs not only enabled rapid protein adsorption, but also decreased the rate of protein elution compared with that of the air-TNTs. We found that the $H_2$-TNTs exhibited better biocompatibility than the air-TNT and Ti groups. Both cell adhesion activity and alkaline phosphatase activity were significantly improved toward MG-63 human osteoblast-like cells as compared with the control groups ($P<0.05$).

**Conclusion:** We conclude that hydrogenated TNTs could greatly improve the loading capacity of bioactive molecules and MG-63 cell proliferation.

**Keywords:** titanium, hydrogenation, nanotubes, hydrophilicity, protein elution, cytocompatibility

## Introduction

Modified titanium (Ti) substrates with titanium dioxide ($TiO_2$) nanotubes (TNTs) have broad usage as implant surface treatment and as drug-delivery systems.[1,2] Their performance in most of these applications is highly dependent on their morphology, nanotube dimension, and wettability. The TNTs increase the surface roughness and wettability of Ti, and their highly effective surface area leads to greater protein adsorption.[3] Previous studies have demonstrated that a diameter of 70–100 nm is the optimum size for bone formation and has been shown to promote macrophage adherence and proliferation, and to inhibit inflammatory cell responses.[4,5] In particular, the increased surface wettability has a stronger immunomodulatory effect than increases in roughness.[6] To further improve the osteogenic properties of $TiO_2$, bioactive molecules can be embedded into the TNTs.[7] The mass of bioactive molecules that can be embedded into the TNTs is determined by the diameter of individual TNTs and their

Correspondence: Su Chen; Zhenting Zhang
Laboratory of Biomaterials and Biomechanics, Beijing Key Laboratory of Tooth Regeneration and Function Reconstruction, School of Stomatology, Capital Medical University, Tian Tan Xi Li No 4, Beijing 100050, People's Republic of China
Tel/fax +86 10 5709 9279
Email dentistchensu@gmail.com; zztttxl@hotmail.com

submit your manuscript | www.dovepress.com
Dovepress
http://dx.doi.org/10.2147/IJN.S155532



© 2018 Lu et al. This work is published and licensed by Dove Medical Press Limited. The full terms of this license are available at https://www.dovepress.com/terms.php and incorporate the Creative Commons Attribution – Non Commercial (unported, v3.0) License (http://creativecommons.org/licenses/by-nc/3.0/). By accessing the work you hereby accept the Terms. Non-commercial uses of the work are permitted without any further permission from Dove Medical Press Limited, provided the work is properly attributed. For permission for commercial use of this work, please see paragraphs 4.2 and 5 of our Terms (https://www.dovepress.com/terms.php).

wettability.[3,8] Larger-diameter TNTs can be loaded with more bioactive molecules, which provide a superhydrophilic surface for liquid and molecules to penetrate.[9] However, wider diameters may cause a larger initial burst release of molecules.[10] Therefore, improving the wettability of TNTs within their range of biocompatibility diameters is of great importance.

Conventional techniques used to improve hydrophilic surfaces such as ultraviolet irradiation[11] and plasma cleaning[12] have been reported to enhance the cell response and promote more rapid osseointegration. Nevertheless, all of these methods have their limitation. Plasma does not penetrate significantly enough into the nanotubes,[2] and a hydrophilic surface achieved by ultraviolet (UV) irradiation depends on the light source power. Only UV light energy greater than 3.2 eV can induce $TiO_2$ photocatalytic activity, which can alter the surface chemistry and enhance hydrophilicity.[13,14] Even if the energy is greater than 3.2 eV, UV–light-induced hydrophilicity may not be very stable.[15] After withdrawal of UV irradiation, the surface wettability will gradually return to the original condition.[16] Thus, in order to improve the photocatalytic effect of $TiO_2$[17,18] and to achieve more stable hydrophilicity by UV irradiation,[11] metal-decorated TNTs were developed. Photocatalysis of metal-decorated $TiO_2$ generated more reactive oxygen species (ROS) and induced a superhydrophilic surface, providing antimicrobial activity and stem cell compatibility.[11,19–21] However, the increase in metallic oxide nanoparticles incorporated into the TNT samples could occupy the binding site of proteins and cause cytotoxicity,[1,22] which may not be good for medical implants and drug-delivery systems.

Recently, hydrogenated $TiO_2$ has been found to generate more –OH species[23] and to offer higher photocatalytic efficiency[24] owing to oxygen vacancies,[25] both of which cause the crystal surface to become superhydrophilic. Both the photocatalytic activity and hydroxyl groups of TNTs are related to implant protein adsorption and biocompatibility with mammalian cells.[11,26,27] However, there have been no in vitro studies analyzing the protein adsorption and biocompatibility of hydrogenated TNTs. Furthermore, reports on hydrogenated TNTs for medical implants (osseointegration and drug delivery) are limited.

The purpose of this study, therefore, was to fabricate superhydrophilic TNTs by thermal hydrogenation and evaluate the adsorption and release of protein from these TNTs. MG-63 human osteoblast-like cells were used to evaluate the biocompatibility and osteogenic effects of different Ti surfaces, because this well-characterized cell line exhibits many osteoblastic traits, which are characteristic of bone-forming cells.[28] The hypothesis of this study is that hydrogenation could improve protein adsorption, prolong the duration of release of effective concentration of protein and accelerate the cell osteogenesis capability. This suggests that the material can potentially be used as a drug-delivery system and as intraosseous implants.

# Materials and methods

## Sample preparation and characterization

### Preparation of TNTs and hydrogenation

The Ti substrates (99.99%; Cuibolin Nonferrous Metal Industry Co., Ltd., Beijing, People's Republic of China, $10\times10\times0.2$ mm$^3$) were ultrasonically washed with acetone, ethyl alcohol, and deionized water for 10 minutes, sequentially. Anodization was conducted in a two-electrode electrochemical cell, where Ti substrates served as the working electrode and a graphite sheet served as the counter electrode at 20°C. The electrolyte was ethylene glycol (with less than 0.5 wt% $H_2O$) containing 0.5 wt% ammonium fluoride ($NH_4F$) and 10 vol% deionized water. After anodization at 50 V for 15 minutes, TNTs were fabricated on the Ti substrates. All samples were rinsed with ethanol and deionized water successively, and annealed at 500°C for 2 hours in air to transform the amorphous TNT phase into a crystalline anatase structure (denoted as air-TNTs), which featured higher corrosion resistance and better biocompatibility than that of the amorphous TNTs.[29,30] The air-TNTs were rinsed with deionized water, dried and sealed in a vacuum quartz tube with $0.95\times10^5$ Pa hydrogen, and then annealed at 500°C for 4 hours to obtain the hydrogenated TNTs (termed $H_2$-TNTs). The Ti substrates were used as a control group. Before in vitro experiments, alcohol-sterilized samples were washed with phosphate-buffered saline (PBS) and then dried out on a clean bench.

## Characterization of samples

The surface morphologies of the Ti, air-TNTs, and $H_2$-TNTs samples were observed with a field-emission scanning electron microscope (SEM, S4800; Hitachi Ltd., Tokyo, Japan) and a transmission electron microscopy (JEOL2011, JEOL. Ltd., Tokyo, Japan). The phase compositions were analyzed by X-ray diffraction (XRD; TTRAX III, Rigaku Co., Tokyo, Japan). The chemical states of the surface constituents were identified by X-ray photoelectron spectroscopy (XPS; ESCALAB 250Xi, Thermo Fisher Scientific, MA, USA). Photoluminescence (PL) characteristics were measured with excitation by a 300-nm laser at room temperature. Contact angle (CA) measurements of the control and experimental samples were carried out with a contact analysis system

(Model OCA15pro, Dataphysics Co., Ltd., Germany). The surface roughness of the samples was measured with an atomic force microscope (AFM; Nanoscope V, Veeco Plainview, NY, USA). The mean surface roughness was calculated for different 10 $\mu m^2$ areas of each sample. The Ra values were expressed as the mean of at least three areas and the SD.

## Protein-binding and elution assay

### Qualitative assessment of protein adsorption in TNTs

To visualize the location of small proteins inside the TNTs, 18-nm diameter colloidal gold-labeled goat antibodies (Jackson ImmunoResearch Laboratories, Inc., USA) were diluted 10 times and used as protein substitutes, dropping onto the TNT surfaces, incubating at 37°C for 30 minutes, and then washing with PBS three times.[8] The surface of the TNTs incubated with the gold-labeled antibodies was mechanically scratched and observed by transmission electron microscopy (TEM; JEOL2011, JEOL. Ltd).

To further investigate the distribution of protein (bovine serum albumin [BSA]; Sigma Aldrich) inside the nanotubes, time-of-flight secondary ion mass spectrometry (TOF-SIMS) was used. Negative depth profiles were recorded on a TOF-SIMS 5-100 instrument (ION-TOF, GmbH, Germany) in dual-beam mode, with a pulsed 60 keV $Bi^+$ liquid-metal ion beam for spectra generation and a 2 keV $Cs^+$ ion beam for sputter-removal. The sputtering speed was 0.313 nm/s for silicon dioxide.

## Protein adsorption assessment

For the Ti, air-TNTs, and $H_2$-TNTs binding experiments, we used BSA (Sigma-Aldrich Co., St Louis, MO, USA), histone from calf thymus (Worthington Biochemical Co., Lakewood, NJ, USA), and fibronectin (FN; Sigma-Aldrich Co) as model proteins. A 200-µL aliquot of protein solution (2 mg/mL BSA, histone or FN) was applied to the samples, and they were incubated at 37°C for 30 minutes. After incubation, a 20-µL aliquot of the supernatant was collected to assess the quantities of unbound proteins. The TNTs/Ti substrates were washed three times with 1 mL PBS to remove weakly bound protein and then were transferred into fresh wells. Then, 200-µL 2% sodium dodecyl sulfate (SDS; Beyotime Institute of Biotechnology Co., Beijing, People's Republic of China) was added to the protein-coated surfaces. Samples were shaken for 2 hours to elute the absorbed protein. The SDS solution with the collected proteins was used for the bound-protein assessment. The concentration of protein was determined with a BCA protein assay kit (Beyotime Institute of Biotechnology Co.). The optical density (OD) at 562 nm was measured with a precision microplate spectrophotometer (SpectraMax Paradigm). Triplicates of three independent samples were measured for each condition.

## Protein elution test

A 50-µL portion of concentrated BSA or histone (10 mg/mL diluted in deionized water) was applied to the surface of the air-TNTs and $H_2$-TNTs. Samples were allowed to dry in a vacuum oven. After drying, the loading procedure was repeated three times. The samples were then gently rinsed with 1 mL PBS to remove the surface layer of protein. Because the drug-release response depends on temperature and pH, we used PBS with a pH of 7.4 at 37°C as the protein-release medium.[31]

The samples were immersed in 200-µL PBS at 37°C in a capped vial and measurements were taken at specified intervals (30 minutes; 1 and 2 hours; 1, 2, 3, 5, and 7 days) by replacing the entire volume of PBS with fresh PBS each time. In vitro release profiles of BSA and histone from the TNTs were evaluated with a micro BCA protein assay kit (Thermo Fisher Scientific, Pierce, Rockford, USA), and the protein concentrations were quantified with a microplate spectrophotometer (SpectraMax Paradigm, Molecular Devices, CA, USA) measuring the OD at 562 nm. Each measurement was conducted in triplicate. After 7 days, all samples were shaken for 2 hours to remove residual protein by 2% SDS. The rate of protein elution was then measured.

## In vitro biocompatibility

### Cell adhesion and proliferation ability assay

The human osteoblastic cell line MG-63 (China Infrastructure of Cell Line Resource, Beijing, People's Republic of China) at passage numbers 3–7 was used in the experiments. The cells were cultured in Dulbecco's Modified Eagle's Medium-Low Glucose (DMEM-LG; Thermo Fisher Scientific, Waltham, MA, USA) in the presence of 10 vol% fetal bovine serum (Thermo Fisher Scientific) and 1 vol% penicillin/streptomycin (PS, Thermo Fisher Scientific). The cell suspension was plated in a cell culture dish and incubated at 37°C under a 5% $CO_2$ atmosphere. Samples were collected in a 50-mL centrifuge tube together with 10-mL cell suspension ($1\times10^5$ cells/mL). The centrifuge tubes were then fixed horizontally to a table concentrator rotating around a fixed axis at a uniform speed in a 37°C incubator. Cell counts in the initial period (1, 2, and 4 hours) were measured to determine the number of cells that adhered to the different samples.

To investigate the proliferation ability of MG-63 on the different samples, a 100-µL portion of cell suspension ($1\times10^5$ cells/mL) was seeded onto each specimen and

incubated in a 5% $CO_2$ incubator for 30 minutes, to allow cells to attach to the sample surfaces. Then, 1 mL of medium was added to each well and further incubated for 1, 3, 5, and 7 days. Cell adhesion and proliferation were measured with a Cell Counting Kit-8 (CCK-8, Dojindo, Japan) according to the manufacturer's instructions.

## MG-63 cell morphology

To investigate the MG-63 shape and orientation at the single-cell level, fluorescence staining microscopy was conducted. MG-63 cells were seeded on the samples in 24-well plates at a density of $1\times10^4$ cells per well for 4 hours. The MG-63 cells that adhered to the samples were fixed with 4% paraformaldehyde at room temperature for 15 minutes. Samples were then washed three times with PBS and permeabilized with 0.2% Triton X-100 at room temperature for 30 minutes. All samples were blocked with 10% goat serum for 30 minutes, and the actin cytoskeletons were labeled by incubating with Alexa Fluor 555 Phalloidin (Cell Signaling Technology, Inc.) for 15 minutes at room temperature in the dark. After rinsing with PBS, the cell nuclei were labeled with DAPI (ZLI-9557, ZSGB-BIO, People's Republic of China) for 5 minutes. Cells were then imaged by confocal laser scanning microscopy (Zeiss 710, Germany).

Furthermore, the morphology of the cells on the samples was observed with the SEM. Cells were seeded in the same manner as indicated earlier. After incubating for 4 hours, all samples were fixed in 2.5% glutaraldehyde for 2 hours at 4°C and then washed three times in PBS for 1 hour. An ethanol concentration gradient of 30, 50, 75, 90, 95, and 100 v/v% was used sequentially to dehydrate the samples. All samples were finally dried to a critical point and sputter coated with gold for observation.

## Alkaline phosphatase activity assay

MG-63 cells were seeded onto the samples at a density of $1\times10^4$ cells per well. The medium was replaced every other day. After culturing for 4 and 7 days, the cells were lysed in a RIPA solution (P0013K, Beyotime Institute of Biotechnology Co.,) by ultrasonication in an ice-water bath. Then, alkaline phosphatase (ALP) activity was assayed by measuring the transformation of p-nitrophenyl-phosphate (pNPP; Beyotime Institute of Biotechnology Co.,) into p-nitrophenol (pNP). The lysate was collected and incubated with 50-µL pNPP solution for 30 minutes at 37°C. The reaction was stopped with 1 N sodium hydroxide (NaOH). The amount of pNP produced was quantified by absorbance measurements at 405 nm and the amount of enzyme released by the cells was quantified by comparison with a standard curve. The intracellular total protein content was determined with the BCA Protein Assay Kit (Beyotime Institute of Biotechnology Co.), and used to normalize the ALP activity.

## Statistical analysis

All data were expressed as the mean ± SD from at least three independent experiments. Data were analyzed by one-way ANOVA combined with the Student–Newman–Keuls post hoc test, or Student's *t*-test using SPSS 20.0 (SPSS, USA). $P<0.05$ was considered to be statistically significant.

# Results

## Sample characterization

The surface morphology and cross-sectional views were observed by SEM for TNT groups (Figure 1). These results showed that the nanotubes in TNT samples were well organized, with diameters of 100 nm and lengths of 1 µm. A longitudinal section of the TNTs from TEM imaging indicated that the internal diameter decreased; however, the outer thickness increased from the top to the bottom of the tube (Figure 2A and B). The well-resolved lattice features, shown in the high-resolution TEM (HRTEM) images (Figure 2a and b), indicate that the air-TNTs were highly crystalline. However, following hydrogenation, a disordered outer layer with a thickness of 2 nm was observed around the crystalline core.

The XRD spectra of the samples displayed Ti and anatase $TiO_2$ peaks in the air-TNT and $H_2$-TNT samples (Figure 3). The anatase peak intensity (as indicated with a black dot) of the $H_2$-TNTs was slightly weakened compared with that of the air-TNTs, suggesting the presence of point defects (oxygen vacancies) in the $TiO_2$ lattice[32] that were induced by the hydrogenation. After hydrogenation, the basic crystal structure was not reformed. Surface roughness values determined from AFM are shown in Table 1. The roughness values of the TNTs surfaces were five times as high as those of the Ti substrates. No major changes in the morphology or roughness were detected through hydrogenation.

## Chemical composition and water contact angle

High-resolution O 1s spectra of the air-TNTs and $H_2$-TNTs are shown in Figure 4. Peaks at 529.9 and 530.4 eV correspond to the characteristic peak of O–Ti.[23,33] After hydrogenation, the atomic percentage of $O_{Ti}$ atoms – determined from fitting to the O 1s peaks – decreased from 84.13% to 64.99%. This significant reduction in the ratio of $O_{Ti}$ indicates the formation of oxygen vacancies during the hydrogenation

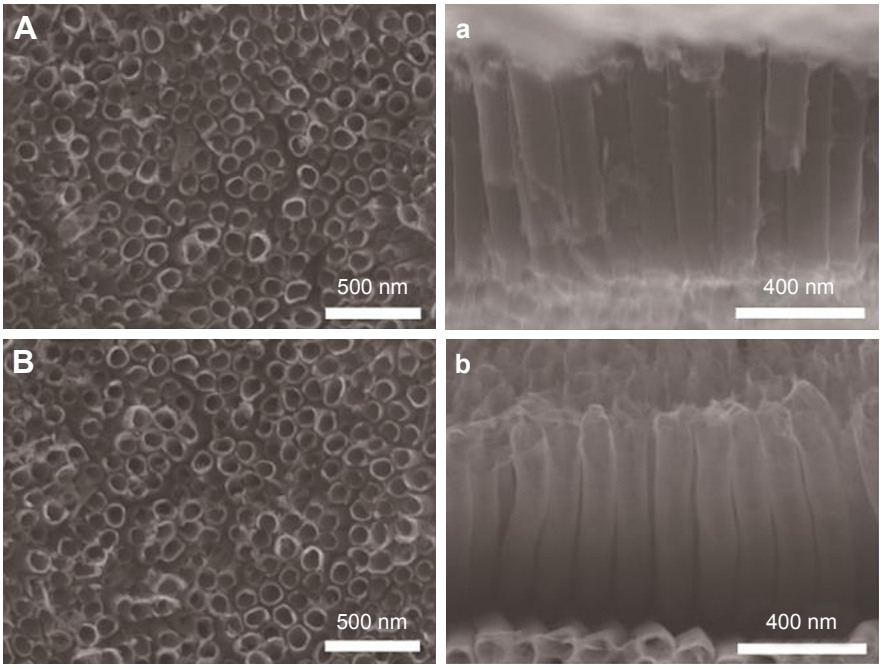



**Figure 1** SEM images of TNTs samples.
**Notes:** (**A**, a) air-TNTs and (**B**, b) $H_2$-TNTs. **A** and **B** show the surface of samples while the a and b show the cross section of samples.
**Abbreviations:** SEM, scanning electron microscopy; air-TNTs, air-annealed $TiO_2$ nanotubes; $H_2$-TNTs, hydrogenated $TiO_2$ nanotubes.

process. Additional peaks centered at 531.4 and 532.0 eV were attributed to hydroxyl species –OH – that is, physically absorbed water.[23,33,34] Note that XPS measurements can only reveal the chemical states of the surface of a material to a depth of a few nanometers. To further investigate the degree of hydrogenation over the whole length (1 μm) of the nanotubes, we also measured PL spectra (Figure 5). After hydrogenation, the relative intensity of the peak clearly increased, suggesting that the concentration of oxygen vacancies increased in the $H_2$-TNTs.[35,36]

The water contact angles are shown in Table 1 and Figure 6. The Ti substrate featured the largest contact angle of 76°. After formation of the air-annealed TNTs, the contact angle decreased to 33°, which was attributed to the reaction products containing hydroxide compounds and due to the TNTs providing space for liquid penetration. The hydrogenation

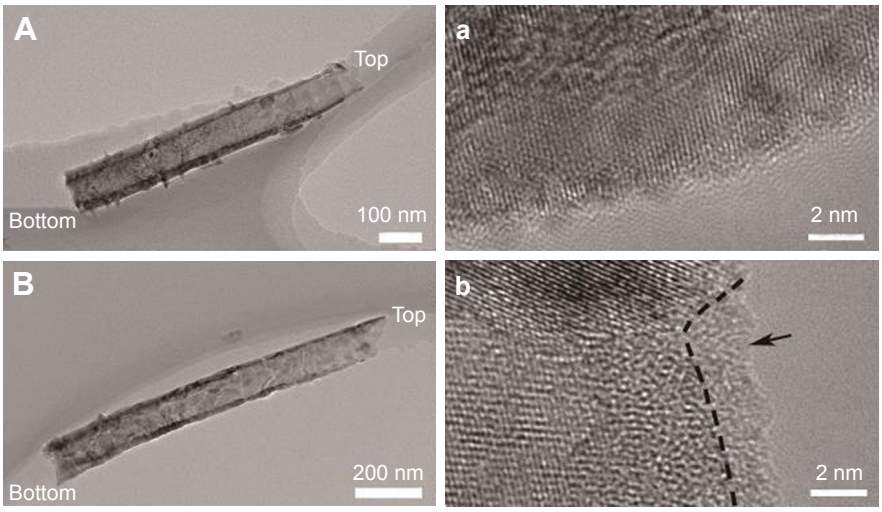



**Figure 2** TEM images of air-TNTs and $H_2$-TNTs.
**Notes:** (**A**, a) air-TNTs and (**B**, b) $H_2$-TNTs. **A** and **B** represent the cross section of samples; a and b represent the high resolution of transmission electron microscopy images of **A** and **B**. In (b), a short dashed curve is applied to outline a portion of the interface between the crystalline and the disordered outer layer (marked by black arrow).
**Abbreviations:** TEM, transmission electron microscopy; air-TNTs, air-annealed $TiO_2$ nanotubes; $H_2$-TNTs, hydrogenated $TiO_2$ nanotubes.

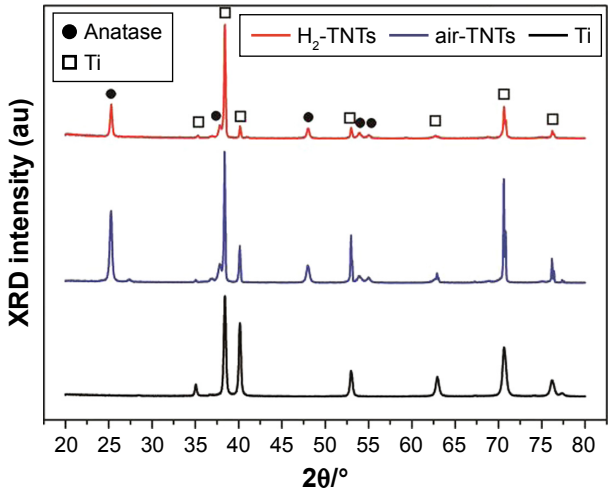



**Figure 3** XRD patterns of Ti substrate, air-TNTs, and $H_2$-TNTs.
**Abbreviations:** XRD, X-ray diffraction; Ti, titanium; air-TNTs, air-annealed $TiO_2$ nanotubes; $H_2$-TNTs, hydrogenated $TiO_2$ nanotubes.

ensured the surface was superhydrophilic with a contact angle of 0°.

## Qualitative assessment of protein adsorption to TNTs

To visualize the small-molecule protein-loading ability of air-TNTs and $H_2$-TNTs, 18-nm diameter colloidal gold-labeled antibodies were used and imaged by TEM. The gold-labeled antibodies could be found both in the interior of air-TNTs (Figure 7A and B) and $H_2$-TNTs (Figure 7C and D), which illustrates that TNTs as a drug-delivery system could trap small proteins inside the nanotubes. To investigate the protein distribution inside the nanostructures, we conducted BSA and sputtering depth profiles (Figure 8) in air-TNTs and $H_2$-TNTs.

**Table 1** Water contact angles and surface roughness of the samples

| Sample | Contact angle (°) | Roughness (nm) |
|---|---|---|
| Ti | 76.0±4.0 | 8.0±3.5 |
| air-TNTs | 33.2±3.2 | 45.8±4.4 |
| $H_2$-TNTs | 3.0±1.0 | 47.6±6.2 |

**Note:** Data are expressed as mean ± SD.
**Abbreviations:** Ti, titanium; air-TNTs, air-annealed $TiO_2$ nanotubes; $H_2$-TNTs, hydrogenated air-TNTs.

The main signals that could be detected were derived from the peptide backbone of proteins and the oxide/metal of the TNTs sample – that is, $CNO^-$, $CN^-$, and $Ti^-$ signals. It shows that, with the increase of sputtering depth, signals from $CNO^-$ and $CN^-$ were at least one order of magnitude higher for the $H_2$-TNTs than those for air-TNTs.

## Quantification of protein adsorption

The binding of BSA, histone, and FN proteins was evaluated on the air-TNTs, $H_2$-TNTs, and the Ti substrate (Figure 9). The lowest quantities of unbound protein (ie, protein in the supernatant) and the highest quantities of bound protein were found for the $H_2$-TNTs samples. FN had the highest absorption capacity as indicated by the concentration of this protein in the supernatants being much lower than that of BSA and histone (Figure 9A). The highest concentration of bound protein after the rinsing step was found for histone (Figure 9B).

## Protein elution test

Figure 10A shows the cumulative amounts of BSA and histone released over time after the immersion of the different samples in PBS. A high rate of release was observed over the first 2 hours, followed by a period of slow and sustained release.

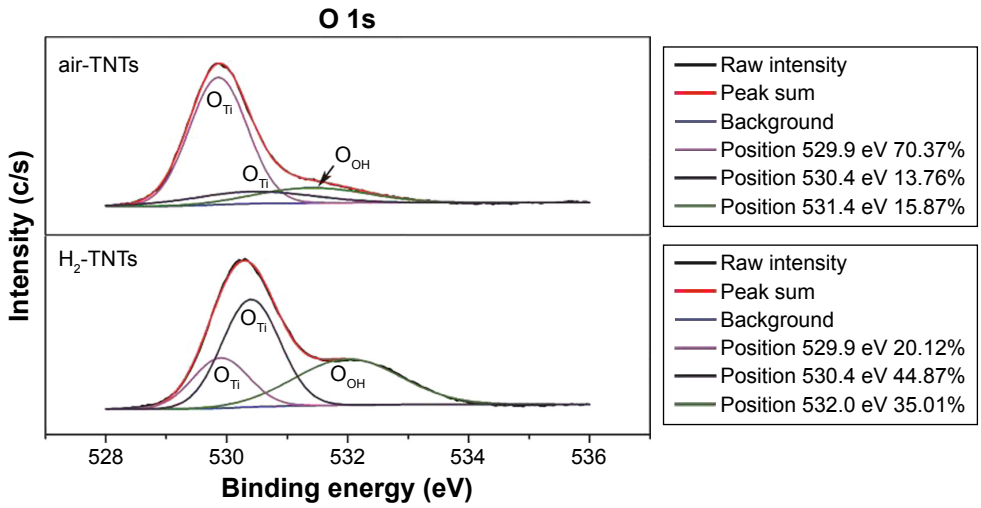



**Figure 4** High-resolution XPS spectra of O 1s.
**Abbreviations:** XPS, X-ray photoelectron spectroscopy; air-TNTs, air-annealed $TiO_2$ nanotubes; $H_2$-TNTs, hydrogenated $TiO_2$ nanotubes.

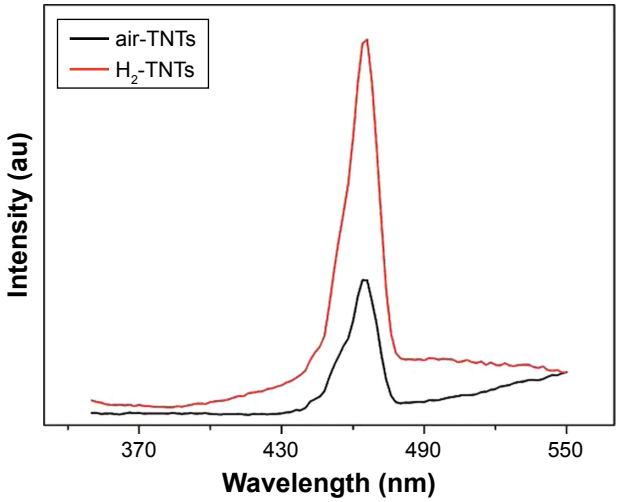



**Figure 5** Photoluminescence characteristics of air-TNTs (black) and $H_2$-TNTs (red).
**Abbreviations:** air-TNTs, air-annealed $TiO_2$ nanotubes; $H_2$-TNTs, hydrogenated $TiO_2$ nanotubes.

The cumulative amount of histone elution was greater than that of BSA. The hydrophilicity of the $H_2$-TNTs decreased the rate of BSA elution over the first 48 hours and that of histone elution in the period after 24 hours (Figure 10B).

## Early cell adhesion and proliferation ability

The adhesion of MG-63 cultured on the different Ti surfaces is shown in Figure 11A. The number of MG-63 cells on the $H_2$-TNTs samples was significantly greater than that of the other groups at all time points ($P<0.05$). The time-dependent proliferation of MG-63 cultured on the samples is shown in Figure 11B. The cell numbers in the three groups increased in a time-dependent manner during the culture period. Cell proliferation on the $H_2$-TNTs surface was greater than that on the air-TNTs and Ti substrates from the third day of incubation ($P<0.05$).

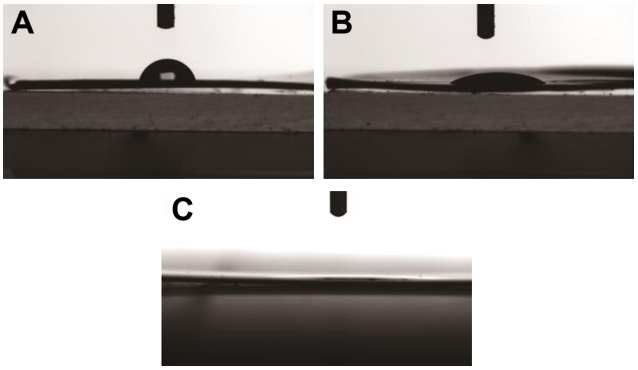



**Figure 6** Water contact angle of (**A**) Ti substrate, (**B**) air-TNTs, and (**C**) $H_2$-TNTs.
**Abbreviations:** Ti, titanium; air-TNTs, air-annealed $TiO_2$ nanotubes; $H_2$-TNTs, hydrogenated $TiO_2$ nanotubes.

## SEM analysis of cell morphology and fluorescence microscopic imaging

The MG-63 cells were cultured for 4 hours. According to SEM imaging (Figure 12), the MG-63 cells appeared to have round and polygonal shapes on the Ti surface. On the $H_2$-TNTs sample, the MG-63 cells had a more elongated shape than those on the air-TNTs. At high magnification, the MG-63 cells featured more pseudopodia on TNTs samples. Fluorescence microscopic images (Figure 13) showed that the morphology of the MG-63 cells on $H_2$-TNTs samples exhibited an extended cytoskeleton at the 4-hour time point.

## ALP activity

The MG-63 ALP activity results are shown in Figure 14. A significant difference between the $H_2$-TNT group and Ti group was observed at Day 4 ($P<0.05$). Furthermore, significant differences were clearly detected by Day 7 among all three groups ($P<0.05$).

# Discussion

This study demonstrated that the thermal hydrogenation of TNTs generated by electrochemical oxidation of Ti can improve the hydrophilicity without changing the morphology. Furthermore, it was found that the increased wettability of the surface in the $H_2$-TNTs sample significantly improved the initial protein adsorption, which is important for promoting osteogenic cell adhesion and differentiation. Moreover, the increased oxygen vacancy and –OH along the whole length of nanotubes in $H_2$-TNTs decrease the rate of protein release. All of this would have profound effects on the drug-delivery system and dental implant materials.

In our study, under similar morphology and roughness, the hydrophilic surface is the most important factor to influence the osseointegration and initial protein adsorption. $H_2$-TNTs had more oxygen vacancy than the air-TNTs, and the oxygen vacancy promoted interactions with water. XPS and PL analyses (Figures 4 and 5) revealed that the area of the $O_{OH}$ peak was more pronounced in $H_2$-TNTs. These results suggest that liquid penetration of TNTs could be improved by thermal hydrogenation. Therefore, more bioactive molecules could become embedded into the TNTs. To test this theory, we conducted protein-binding and elution assays. Predictably, protein substitutes could be found both in the interior of air-TNTs and $H_2$-TNTs, and the TOF-SIMS also confirmed that the $H_2$-TNTs featured a higher capacity for adsorbing BSA proteins inside the nanotubes (Figures 7 and 8). A previous study on molecular dynamics simulations have shown that the $TiO_2$ (110) surface modified

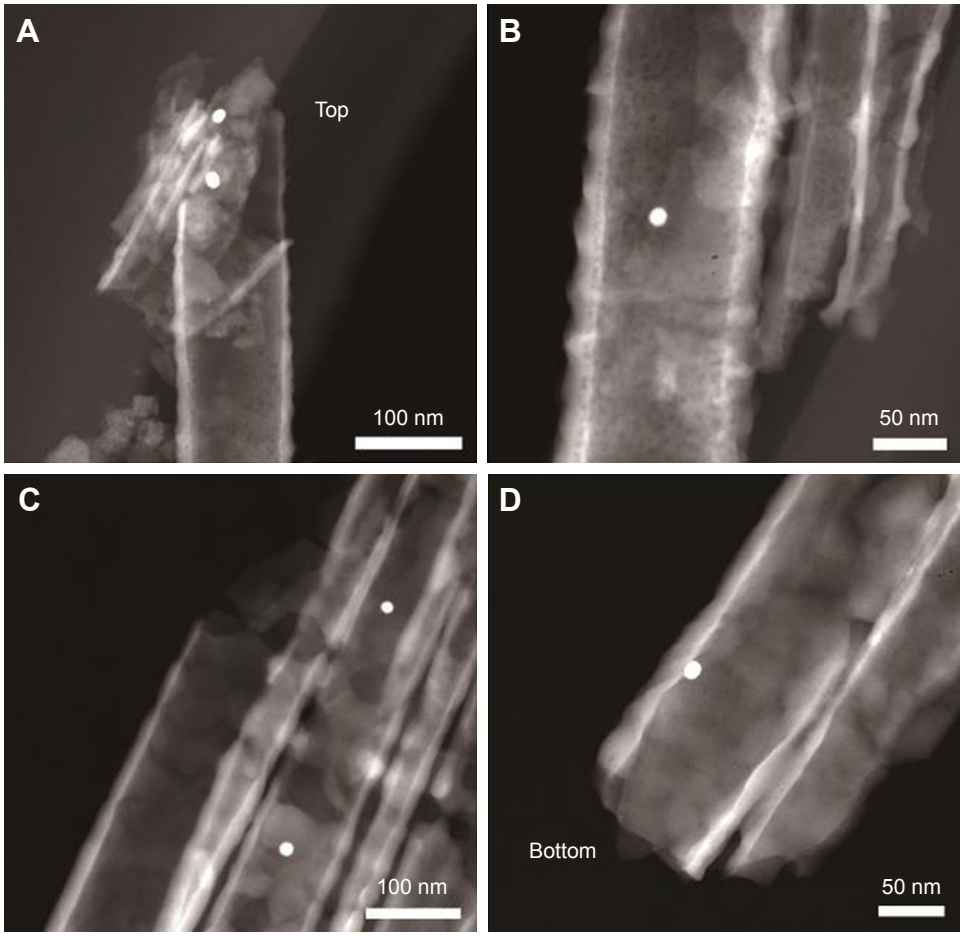



**Figure 7** Gold-labeled antibodies inside (**A**, **B**) air-TNTs and (**C**, **D**) $H_2$-TNT.
**Note:** The gold-labeled antibodies localized in the upper and middle sections of the air-TNTs (**A**, **B**), and penetrated deeper into the $H_2$-TNTs (**C**, **D**).
**Abbreviations:** air-TNTs, air-annealed $TiO_2$ nanotubes; $H_2$-TNTs, hydrogenated $TiO_2$ nanotubes.

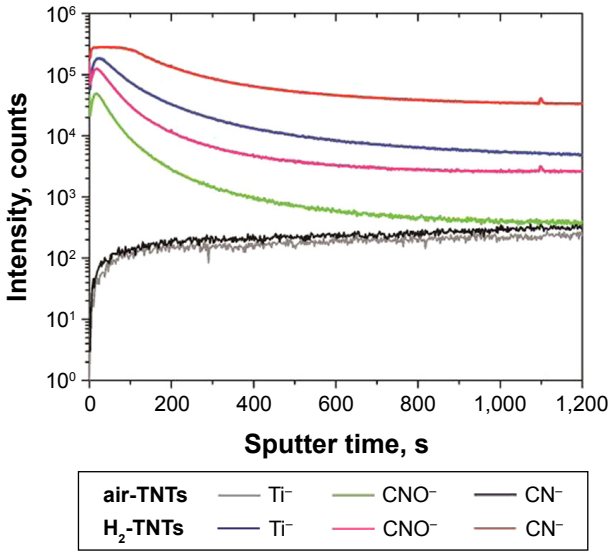



**Figure 8** Negative TOF-SIMS sputter depth profiles for air-TNTs and $H_2$-TNTs treated with BSA.
**Abbreviations:** TOF-SIMS, time-of-flight secondary ion mass spectrometry; air-TNTs, air-annealed $TiO_2$ nanotubes; $H_2$-TNTs, hydrogenated $TiO_2$ nanotubes; BSA, bovine serum albumin.

with –OH groups features a much greater affinity for human serum albumin, reflected by stronger protein-surface electrostatic interactions and a greater number of adsorbed residues.[37] Such small, bioactive, molecule-binding behavior makes this hydrogenated TNT material a more effective drug-delivery carrier compared to air-TNTs.

Different protein-binding assays (Figure 9A) showed that the FN had the highest absorption capacity, indicated by the protein concentration in the supernatants being much lower than that of BSA and histone. FN is a macromolecular glycoprotein with a length 60 nm and radius 6 nm,[38] which might have more binding sites to facilitate deposition on the sample surface. Furthermore, the isoelectric point of FN ranges from 5.6 to 6.1, which is very close to the physiological pH.[39] It has been reported that protein molecules show the highest surface activity and are generally adsorbed most readily to surfaces when their pH is close to the isoelectric point of the surface.[40] However, most of the FN was lost during rinsing as the high-molecular-weight macromolecule FN

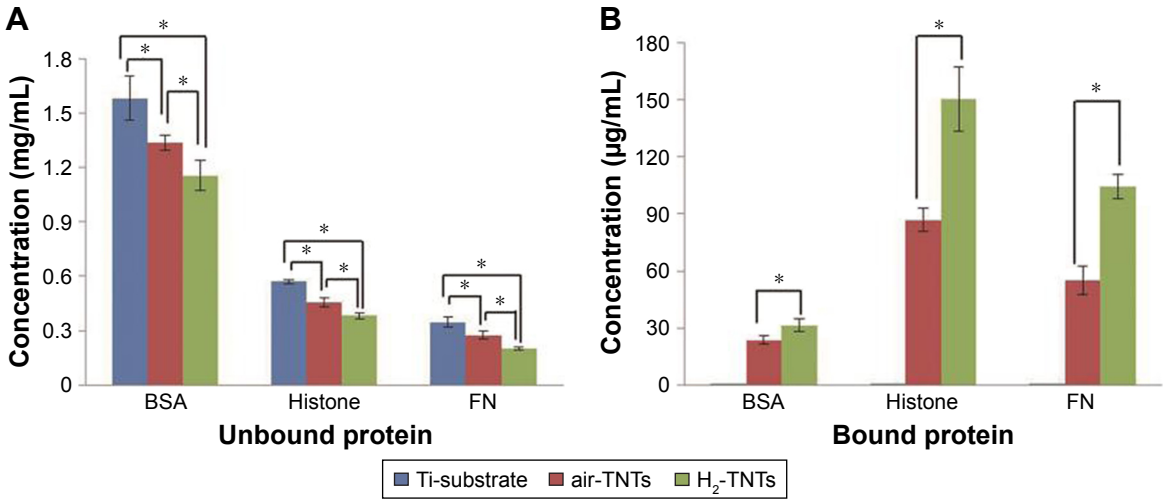



**Figure 9** (**A**) Unbound and (**B**) bound protein on Ti substrate, air-TNTs, and $H_2$-TNTs after incubation for 30 minutes.
**Notes:** Data are expressed as the mean ± SD; (n=3); *$P<0.05$.
**Abbreviations:** Ti, titanium; air-TNTs, air-annealed $TiO_2$ nanotubes; $H_2$-TNTs, hydrogenated $TiO_2$ nanotubes; BSA, bovine serum albumin; FN, fibronectin.

barely assembled into the nanotubes. This can explain why the highest concentration of bound protein after the rinsing step was constituted by histone (Figure 9B). TNTs have a pocket effect for small molecules. Both BSA and histone have a hydrodynamic radius of approximately 7–8 nm[8,41] and, once trapped inside the nanotubes, they are difficult to remove by rinsing. Considering the positive charge of histone (isoelectric point [IEP]=11)[3] and the negative charge of BSA (IEP=4.7),[42,43] histone is expected to have a stronger bonding with the negatively charged Ti substrate and TNTs.[44] The release profiles were similar for histone and BSA, although a slower release and higher cumulative amount was achieved by histone (Figure 10). This phenomenon might be because of the strong electrostatic interaction between the histone and TNTs. In consideration of the pocket effect of TNTs, we only studied BSA and histone as a model to evaluate the protein elution.

A previous study found that plasma treatment decreased the rate of drug elution but did not improve the cumulative release amount of the drug.[2] However, in our study, $H_2$-TNTs not only decreased the rate of BSA elution over the first 48 hours but also increased the cumulative release amount of BSA. It is possible that the hydrogenation penetrates significantly deeper into the tubes, which could trap more BSA protein. Owing to the lower rate of protein elution (positive protein) and higher release cumulative amount (negative protein), $H_2$-TNTs might provide more sustained release over an extended period of time and a higher biological activity than what is possible with the air-TNTs. It has been shown that cationic antimicrobial peptides present broad antimicrobial

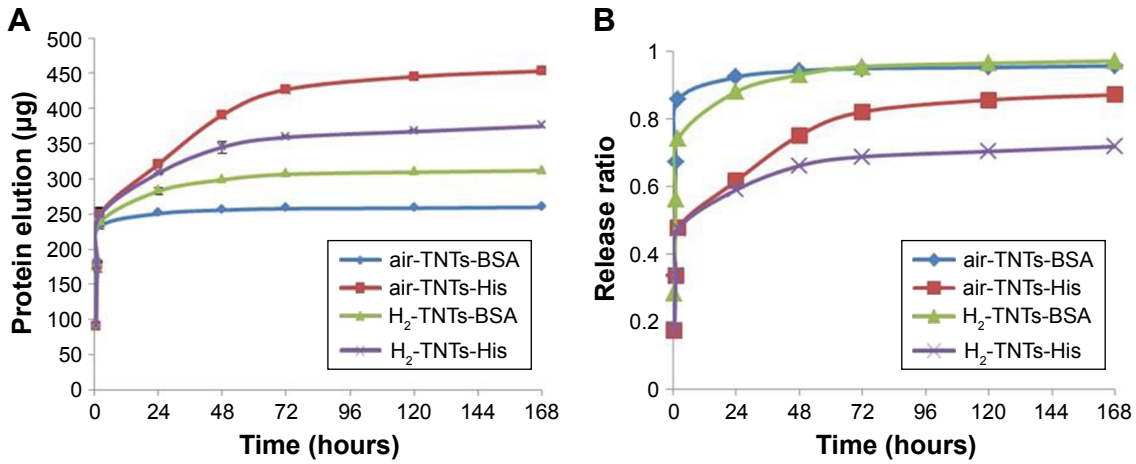



**Figure 10** (**A**) Accumulated protein release, and (**B**) protein release concentrations/total protein concentrations of TNTs samples.
**Notes:** Data are expressed as mean ± SD; (n=3).
**Abbreviations:** air-TNTs, air-annealed $TiO_2$ nanotubes; His, histone; $H_2$-TNTs, hydrogenated $TiO_2$ nanotubes; BSA, bovine serum albumin.

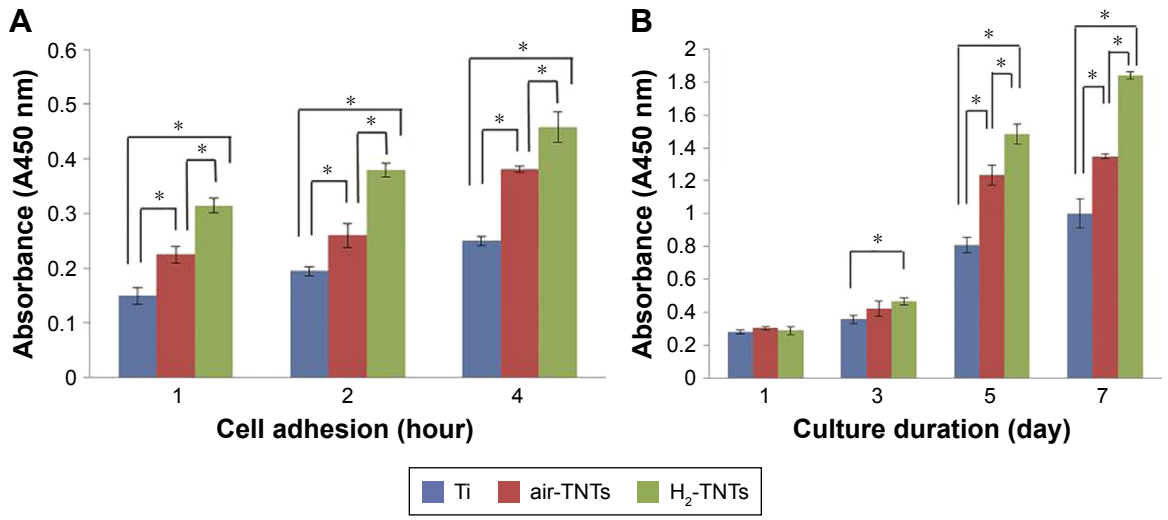



**Figure 11** (**A**) CCK-8 results of MG-63 cell adhesion on samples over 1, 2, and 4 hours. (**B**) CCK-8 results of MG-63 cell proliferation on samples after 1, 3, 5, and 7 days.
**Notes:** Data are expressed as mean ± SD (n=3); *$P<0.05$.
**Abbreviations:** CCK-8, Cell Counting Kit-8; Ti, titanium; air-TNTs, air-annealed $TiO_2$ nanotubes; $H_2$-TNTs, hydrogenated $TiO_2$ nanotubes.

activity without inducing the development of resistant bacteria.[45,46] In this case, the hydrogenated TNTs may have a wide application prospect for prolonging the time of antibacterial activities as well as reducing the cytotoxicity.

Notably, more protein was adsorbed by the $H_2$-TNTs than by the air-TNTs, despite the charge of protein (Figure 9). This result was attributed to the superhydrophilic surface induced by hydrogenation. It has been reported that albumin and FN are beneficial proteins for absorption onto biomaterials and mediate a variety of cellular interactions within the extracellular matrix, playing an important role in antibacterial properties and cell adhesion.[47,48] In our study, more BSA and FN were adsorbed by the $H_2$-TNTs than the air-TNTs, which might influence osteoblast formation and accelerate bone integration. The cell morphology observed by SEM (Figure 12) and fluorescence microscopy (Figure 13) demonstrated that, compared to MG-63 cells on the Ti and air-TNTs surface, the MG-63 cells on the surface of $H_2$-TNTs had elongated morphology with more widespread filopodia and regular arrangement of an

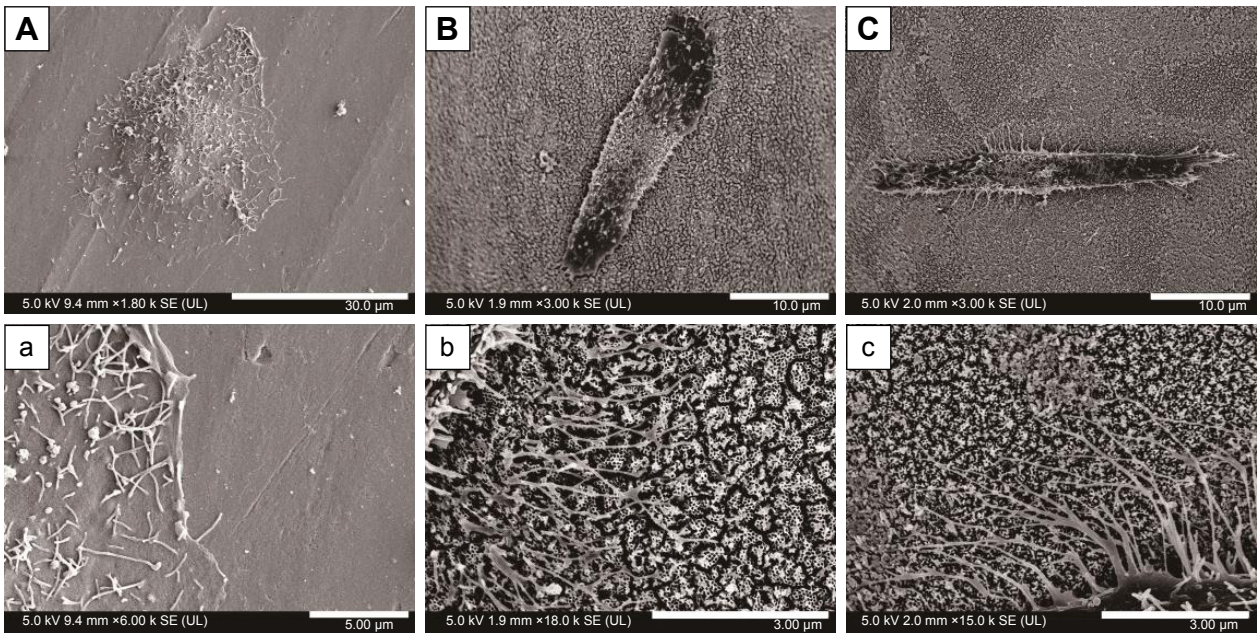



**Figure 12** SEM images of MG-63 cell on samples after culturing for 4 hours: (**A**, a) Ti substrate, (**B**, b) air-TNTs, and (**C**, c) $H_2$-TNTs.
**Note:** Figures a–c show figures **A**–**C** at high magnification, respectively.
**Abbreviations:** SEM, scanning electron microscopy; Ti, titanium; air-TNTs, air-annealed $TiO_2$ nanotubes; $H_2$-TNTs, hydrogenated $TiO_2$ nanotubes.

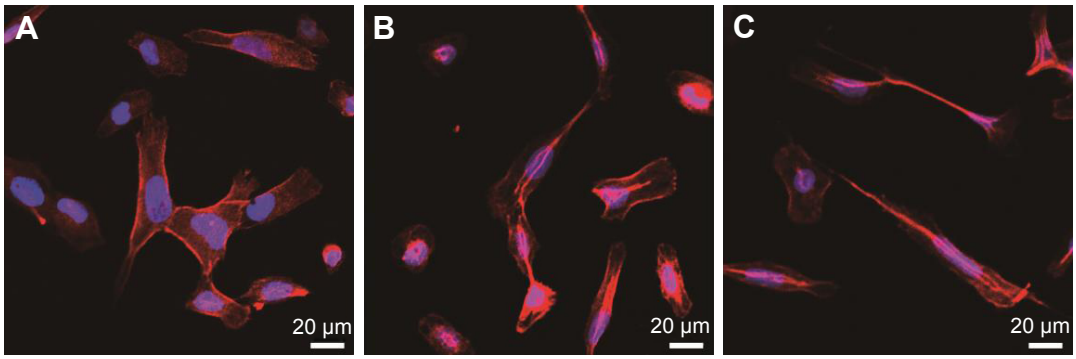



**Figure 13** Fluorescence microscopy of MG-63 cells cultured for 4 hours on (**A**) Ti substrates, (**B**) air-TNTs, and (**C**) $H_2$-TNTs. Actin is shown in red and cell nucleus is shown in blue.
**Abbreviations:** Ti, titanium; air-TNTs, air-annealed $TiO_2$ nanotubes; $H_2$-TNTs, hydrogenated $TiO_2$ nanotubes.

actin cytoskeleton. An elongated shape has been shown to be beneficial to osteoblast differentiation. Previous studies have shown that physical stresses from nanotube topography can regulate cell morphology and accelerate cell differentiation.[49] On larger-diameter nanotubes (100 nm), human mesenchymal stem cells are stressed and forced to elongate, and when stem cells are stressed and elongated, they tend to differentiate into a specific lineage to accommodate the stress.[50] This elongated cell forms were more evident in metal-decorated (eg, Sr and Zn) TNTs and hydrophilic TNTs.[1,11,51] In our study, the cellular cytoskeletal tension and stress in elongated MG-63 cells on $H_2$-TNTs might promote MG-63 differentiation into a more bone-like phenotype,[12,26] which was further confirmed by the ALP activity assay.

Furthermore, ALP is widely used as an early differentiation marker of osteoblasts, which participate in the process of pre-mineralization and promote the formation of mineral nodules.[52] The significantly higher ALP values for the $H_2$-TNTs group after 4 and 7 days suggest that the hydrogenated surface and its higher protein adsorption enhance ALP activity and early cell differentiation (Figure 14). This result is in good agreement with the imaging by SEM and of the cytoskeletal stain. Hydrogenation could improve the wettability and protein adsorption of the TNTs, which is important for the early bone osseointegration effect.

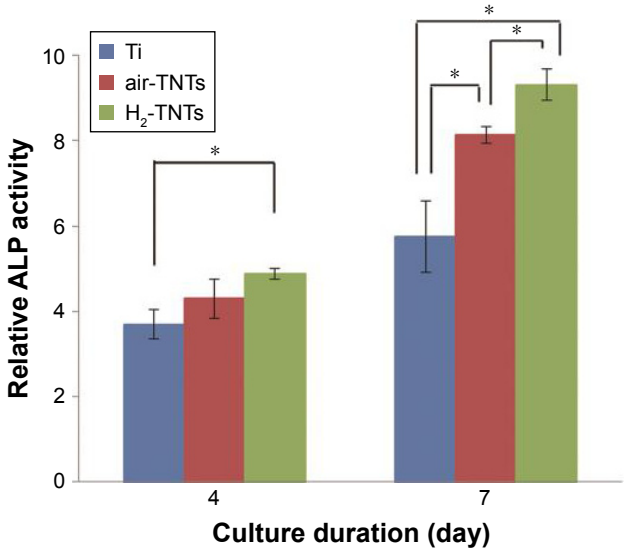



**Figure 14** MG-63 cell ALP activity on samples after incubation for 4 and 7 days.
**Notes:** Data are expressed as mean ± SD (n=3); *$P<0.05$.
**Abbreviations:** ALP, alkaline phosphatase; Ti, titanium; air-TNTs, air-annealed $TiO_2$ nanotubes; $H_2$-TNTs, hydrogenated $TiO_2$ nanotubes.

## Conclusion

Thermal hydrogenation improved both the wettability and protein adsorption of TNTs. Hydrogenated TNTs can potentially be applied as drug carriers, owing to their ability to sustain the release of an effective concentration of protein over an extended period of time. Due to the nanotopography of the TNTs and superhydrophilic surface induced by hydrogenation, the cell compatibility of the $H_2$-TNTs was improved. Moreover, our results showed that MG-63 promoted more filopodia extension on the $H_2$-TNTs, which then enhanced osteogenic cell function and accelerated osteogenic potential at the protein level.

The hydrogenated TNTs used in this study were capable of trapping relatively small amounts of protein and to facilitate the FN deposition. Improvements in drug-loading capacity, extension of the elution duration, and promotion of cell proliferation are the advantages that this material and technology can be applied for in the clinical setting.

## Acknowledgments

The authors gratefully acknowledge financial support from the National Natural Science Foundation of China (grant nos 81570999, 51771098, and u1430118) and the Science Challenge Project (grant no tz2016004).

## Disclosure

The authors report no conflicts of interest in this work.

## References


1. Liu W, Su P, Chen S, et al. Synthesis of TiO2 nanotubes with ZnO nanoparticles to achieve antibacterial properties and stem cell compatibility. *Nanoscale*. 2014;6(15):9050–9062.
2. Peng L, Mendelsohn AD, LaTempa TJ, Yoriya S, Grimes CA, Desai TA. Long-term small molecule and protein elution from TiO2 nanotubes. *Nano Lett*. 2009;9(5):1932–1936.
3. Kulkarni M, Flašker A, Lokar M, et al. Binding of plasma proteins to titanium dioxide nanotubes with different diameters. *Int J Nanomedicine*. 2015;10:1359–1373.
4. Wang N, Li H, Lü W, et al. Effects of TiO2 nanotubes with different diameters on gene expression and osseointegration of implants in minipigs. *Biomaterials*. 2011;32(29):6900–6911.
5. Lü WL, Wang N, Gao P, Li CY, Zhao HS, Zhang ZT. Effects of anodic titanium dioxide nanotubes of different diameters on macrophage secretion and expression of cytokines and chemokines. *Cell Prolif*. 2015; 48(1):95–104.
6. Hotchkiss KM, Reddy GB, Hyzy SL, Schwartz Z, Boyan BD, Olivares-Navarrete R. Titanium surface characteristics, including topography and wettability, alter macrophage activation. *Acta Biomater*. 2016; 31:425–434.
7. Ma Y, Zhang Z, Liu Y, et al. Nanotubes functionalized with BMP2 knuckle peptide improve the osseointegration of titanium implants in rabbits. *J Biomed Nanotechnol*. 2015;11(2):236–244.
8. Kulkarni M, Mazare A, Park J, et al. Protein interactions with layers of TiO2 nanotube and nanopore arrays: morphology and surface charge influence. *Acta Biomater*. 2016;45:357–366.
9. Liu G, Du K, Wang K. Surface wettability of TiO2 nanotube arrays prepared by electrochemical anodization. *Appl Surf Sci*. 2016;388: 313–320.
10. Liang K, Li X, Tay BK. Fabrication of large diameter TiO2 nanotube for bone morphogenetic protein-2 delivery. *Int J Nanotechnol*. 2014;11(12): 1097–1109.
11. Liu W, Su P, Chen S, et al. Antibacterial and osteogenic stem cell differentiation properties of photoinduced TiO2 nanoparticle-decorated TiO2 nanotubes. *Nanomedicine (Lond)*. 2015;10(5):713–723.
12. Duske K, Koban I, Kindel E, et al. Atmospheric plasma enhances wettability and cell spreading on dental implant metals. *J Clin Periodontol*. 2012;39(4):400–407.
13. Aita H, Att W, Ueno T, et al. Ultraviolet light-mediated photofunctionalization of titanium to promote human mesenchymal stem cell migration, attachment, proliferation and differentiation. *Acta Biomater*. 2009;5(8):3247–3257.
14. Rana S, Rawat J, Misra RD. Anti-microbial active composite nanoparticles with magnetic core and photocatalytic shell: TiO2-NiFe2O4 biomaterial system. *Acta Biomater*. 2005;1(6):691–703.
15. Lorenzetti M, Bernardini G, Luxbacher T, Santucci A, Kobe S, Novak S. Surface properties of nanocrystalline TiO2 coatings in relation to the in vitro plasma protein adsorption. *Biomed Mater*. 2015;10(4):045012.
16. Wang R, Hashimoto K, Fujishima A, et al. Light-induced amphiphilic surfaces. *Nature*. 1997;388(6641):431–432.
17. Sunkara BK, Misra RD. Enhanced antibactericidal function of W4+−doped titania-coated nickel ferrite composite nanoparticles: a biomaterial system. *Acta Biomater*. 2008;4(2):273–283.
18. Rana S, Rawat J, Sorensson MM, Misra RD. Antimicrobial function of Nd 3+−doped anatase titania-coated nickel ferrite composite nanoparticles: a biomaterial system. *Acta Biomater*. 2006;2(4):421–432.
19. Venkatasubramanian R, Srivastava RS, Misra RDK. Comparative study of antimicrobial and photocatalytic activity in titania encapsulated composite nanoparticles with different dopants. *Mater Sci Technol*. 2008;24(5):589–595.
20. Rawat J, Rana S, Srivastava R, Misra RD. Antimicrobial activity of composite nanoparticles consisting of titania photocatalytic shell and nickel ferrite magnetic core. *Mater Sci Eng C*. 2007;27(3):540–545.
21. Rawat J, Rana S, Sorensson MM, Misra RDK. Anti-microbial activity of doped anatase titania coated nickel ferrite composite nanoparticles. *Mater Sci Technol*. 2007;23(1):97–102.
22. Liu W, Su P, Gonzales A 3rd, et al. Optimizing stem cell functions and antibacterial properties of TiO2 nanotubes incorporated with ZnO nanoparticles: experiments and modeling. *Int J Nanomedicine*. 2015;10:1997–2019.
23. Lu X, Wang G, Zhai T, et al. Hydrogenated TiO2 nanotube arrays for supercapacitors. *Nano Lett*. 2012;12(3):1690–1696.
24. Li H, Chen Z, Tsang CK, et al. Electrochemical doping of anatase TiO2 in organic electrolytes for high-performance supercapacitors and photocatalysts. *J Mater Chem A*. 2014;2(1):229–236.
25. Chen X, Liu L, Yu PY, Mao SS. Increasing solar absorption for photocatalysis with black hydrogenated titanium dioxide nanocrystals. *Science*. 2011;331(6018):746–750.
26. Zhao G, Schwartz Z, Wieland M, et al. High surface energy enhances cell response to titanium substrate microstructure. *J Biomed Mater Res A*. 2005;74(1):49–58.
27. Li S, Ni J, Liu X, et al. Surface characteristics and biocompatibility of sandblasted and acid-etched titanium surface modified by ultraviolet irradiation: an in vitro study. *J Biomed Mater Res B Appl Biomater*. 2012;100(6):1587–1598.
28. Rausch-fan X, Qu Z, Wieland M, Matejka M, Schedle A. Differentiation and cytokine synthesis of human alveolar osteoblasts compared to osteoblast-like cells (MG63) in response to titanium surfaces. *Dent Mater*. 2008;24(1):102–110.
29. Huang Q, Yang Y, Hu R, Lin C, Sun L, Vogler EA. Reduced platelet adhesion and improved corrosion resistance of superhydrophobic TiO2-nanotube-coated 316L stainless steel. *Colloids Surf B Biointerfaces*. 2015;125:134–141.
30. Huang Q, Yang Y, Zheng D, et al. Effect of construction of TiO2 nanotubes on platelet behaviors: structure-property relationships. *Acta Biomater*. 2017;51:505–512.
31. Zhang J, Misra RD. Magnetic drug-targeting carrier encapsulated with thermosensitive smart polymer: core-shell nanoparticle carrier and drug release response. *Acta Biomater*. 2007;3(6):838–850.
32. Liu N, Häublein V, Zhou X, et al. "Black" TiO2 nanotubes formed by high-energy proton implantation show noble-metal-co-catalyst free photocatalytic H2-evolution. *Nano Lett*. 2015;15(10):6815–6820.
33. Shao S, Dimitrov M, Guan N, Köhn R. Crystalline nanoporous metal oxide thin films by post-synthetic hydrothermal transformation: SnO2 and TiO2. *Nanoscale*. 2010;2(10):2054–2057.
34. Wang G, Wang H, Ling Y, et al. Hydrogen-treated TiO2 nanowire arrays for photoelectrochemical water splitting. *Nano Lett*. 2011;11(7): 3026–3033.
35. Pan X, Yang MQ, Fu X, Zhang N, Xu YJ. Defective TiO2 with oxygen vacancies: synthesis, properties and photocatalytic applications. *Nanoscale*. 2013;5(9):3601–3614.
36. Khan MM, Ansari SA, Pradhan D, et al. Band gap engineered TiO2 nanoparticles for visible light induced photoelectrochemical and photocatalytic studies. *J Mater Chem A*. 2014;2(3):637–644.
37. Kang Y, Li X, Tu Y, Wang Q, Ågren H. On the mechanism of protein adsorption onto hydroxylated and nonhydroxylated TiO2 surfaces. *J Phys Chem C*. 2010;114(34):14496–14502.
38. Lhoest JB, Detrait E, van den Bosch de Aguilar P, Bertrand P. Fibronectin adsorption, conformation, and orientation on polystyrene substrates studied by radiolabeling, XPS, and ToF SIMS. *J Biomed Mater Res*. 1998;41(1):95–103.
39. Boughton BJ, Simpson AW. The biochemical and functional heterogeneity of circulating human plasma fibronectin. *Biochem Biophys Res Commun*. 1984;119(3):1174–1180.
40. Zawala J, Todorov R, Olszewska A, Exerowa D, Malysa K. Influence of pH of the BSA solutions on velocity of the rising bubbles and stability of the thin liquid films and foams. *Adsorption*. 2010;16(4–5):423–435.
41. Hiemstra C, Zhong Z, van Steenbergen MJ, Hennink WE, Feijen J. Release of model proteins and basic fibroblast growth factor from in situ forming degradable dextran hydrogels. *J Control Release*. 2007;122(1): 71–78.
42. Roessler S, Zimmermann R, Scharnweber D, Werner C, Worch H. Characterization of oxide layers on Ti6Al4V and titanium by streaming potential and streaming current measurements. *Colloids Surf B Biointerfaces*. 2002;26(4):387–395.

43. Ge S, Kojio K, Takahara A, Kajiyama T. Bovine serum albumin adsorption onto immobilized organotrichlorosilane surface: influence of the phase separation on protein adsorption patterns. *J Biomater Sci Polym Ed*. 1998;9(2):131–150.
44. Wang T, Liu W, Xu N, Ni J. Adsorption and desorption of Cd(II) onto titanate nanotubes and efficient regeneration of tubular structures. *J Hazard Mater*. 2013;250–251:379–386.
45. Hancock RE. Cationic peptides: effectors in innate immunity and novel antimicrobials. *Lancet Infect Dis*. 2001;1(3):156–164.
46. Li T, Wang N, Chen S, Lu R, Li H, Zhang Z. Antibacterial activity and cytocompatibility of an implant coating consisting of TiO2 nanotubes combined with a GL13K antimicrobial peptide. *Int J Nanomedicine*. 2017;12:2995–3007.
47. Kinnari TJ, Peltonen LI, Kuusela P, Kivilahti J, Könönen M, Jero J. Bacterial adherence to titanium surface coated with human serum albumin. *Otol Neurotol*. 2005;26(3):380–384.
48. Widhe M, Shalaly ND, Hedhammar M. A fibronectin mimetic motif improves integrin mediated cell biding to recombinant spider silk matrices. *Biomaterials*. 2016;74:256–266.
49. Wang N, Li H, Wang J, Chen S, Ma Y, Zhang Z. Study on the anticorrosion, biocompatibility, and osteoinductivity of tantalum decorated with tantalum oxide nanotube array films. *ACS Appl Mater Interfaces*. 2012;4(9):4516–4523.
50. Oh S, Brammer KS, Li YS, et al. Stem cell fate dictated solely by altered nanotube dimension. *Proc Natl Acad Sci U S A*. 2009;106(7):2130–2135.
51. Zhao L, Wang H, Huo K, et al. The osteogenic activity of strontium loaded titania nanotube arrays on titanium substrates. *Biomaterials*. 2013;34(1):19–29.
52. Olivares-Navarrete R, Hyzy SL, Hutton DL, et al. Direct and indirect effects of microstructured titanium substrates on the induction of mesenchymal stem cell differentiation towards the osteoblast lineage. *Biomaterials*. 2010;31(10):2728–2735.



**International Journal of Nanomedicine**

Dovepress

## Publish your work in this journal

The International Journal of Nanomedicine is an international, peer-reviewed journal focusing on the application of nanotechnology in diagnostics, therapeutics, and drug delivery systems throughout the biomedical field. This journal is indexed on PubMed Central, MedLine, CAS, SciSearch®, Current Contents®/Clinical Medicine, Journal Citation Reports/Science Edition, EMBase, Scopus and the Elsevier Bibliographic databases. The manuscript management system is completely online and includes a very quick and fair peer-review system, which is all easy to use. Visit http://www.dovepress.com/testimonials.php to read real quotes from published authors.

**Submit your manuscript here:** http://www.dovepress.com/international-journal-of-nanomedicine-journal